Appl. Phys. B 32, 175–186 (1983)

Applied Physics B Photophysics and Laser Chemistry

Investigation of Stimulated Brillouin Scattering Under Well-Defined Interaction Conditions

Part I. Experimental Basis

B. Gellert* and B. Kronast

Institut für Experimentalphysik V, Ruhruniversität, D-4630 Bochum, Fed. Rep. Germany

Received 18 May 1983/Accepted 22 August 1983

Abstract. Ruby-laser light scattering was used to gain spatially and temporally resolved information about plasma parameters for nanosecond CO_2 laser-plasma interaction studies. The results confirm a heating model, where heat conduction in dense model plasmas can be described classically. CO_2-laser excited stimulated Brillouin scattering could directly be shown to arise from near thermal level by simultaneous Thomson scattering with a ruby-laser, and turbulence enhanced density fluctuations could be excluded.

PACS: 52.25F, 52.25P, 52.35

A large variety of targets has been used in laser-fusion experiments. At present state, it seems necessary to use targets of millimeter diameter and laser-pulse durations of several nanoseconds. The corona surrounding these targets represents an underdense and rather homogeneous plasma of even larger extension, featuring just those conditions for which strong Stimulated Brillouin Scattering (SBS) is anticipated theoretically [1]. The maximum backscattering according to the Manley-Rowe relations may reach near 100% for such conditions.

In spite of a multitude of respective experiments [2–6] this Manley-Rowe limit could be demonstrated so far in a single experiment [7] only. The reason for this singularity most likely is to be sought in the deliberate intention of the experiment to provide for laser and plasma conditions such as they are stipulated in the above theoretical treatments. In a first comparison between experiment and theory [7, 8] the SBS features at, and near threshold could be shown to correspond to the theoretical predictions. The heating model developed in [8] is capable to explain the wide scatter in data reported to date. Trying to understand the SBS behaviour also well above threshold, it was found, that, in addition to plasma parameters such as they were determined in [7, 8a, 8b], drifts of electrons and ions, initial and final amplitudes of ion accoustic waves and also the extension of the interaction volume must be known – for details even their time dependence.

Whereas in many published experiments the plasma parameters of the SBS interaction volume had to be estimated theoretically, this paper gives the results of direct measurements of the corresponding parameters in the plasma, where a well-defined SBS experiment is performed. It was not intended to study the Z-pinch itself, e.g. its dynamics to check various Z-pinch models.

In order to measure the required quantities, there is no better method than light scattering with another laser, for instance a ruby-laser. A comparison with the data obtained from an interpretation of SBS features in [7, 8a, 8b] leads to an independent confirmation of the results and views derived. Over and above, it is the main purpose of this paper to lay a major part of the experimental groundwork required for an explanation of SBS behaviour well above threshold as it will be dealt with in a forthcoming paper [9b].

1. Experimental Set-Up

In order to guarantee well-defined plasma conditions from the very beginning of interaction, a plasma was

* *Present address:* Brown Boveri & Cie, Research Centre, CH-5405 Baden-Dättwil, Switzerland

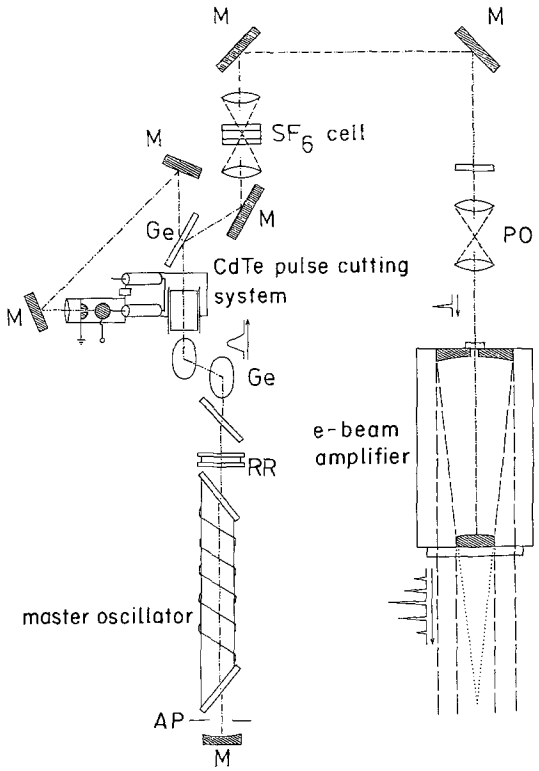

Fig. 1. Schematic set-up of CO_2-laser system consisting of master oscillator, CdTe pulse cutting system with laser triggered spark gap SF_6 cell, and e-beam controlled amplifier (M: mirror, Ge: germanium plates of Brewster angle polarizor, RR: resonance reflector for stable emission of $P20$ transition at 10.6 µm, AP: aperture, forcing emission in TEM_{00}-mode, PO: protection optics)

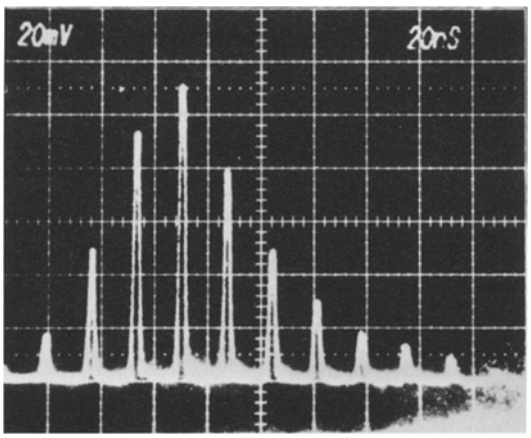

Fig. 2. Temporal development of CO_2 laser emission (horizontal scale 20 ns/division, vertical scale 20 mV/division ≙ 1 GW/division)

used which was preformed in a dynamic Z-pinch device. Since this target plasma was described in great detail in [7] it will suffice here to summarize its features. The plasma column of about 18 mm diameter was homogeneous in density and temperature within 10–20% over about 16 mm diameter with space and

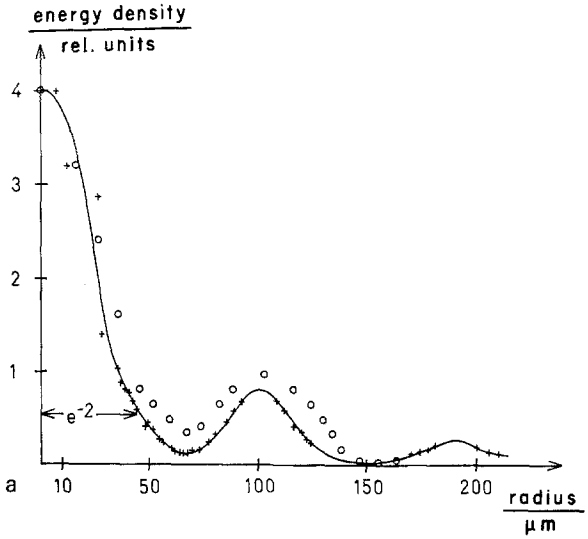

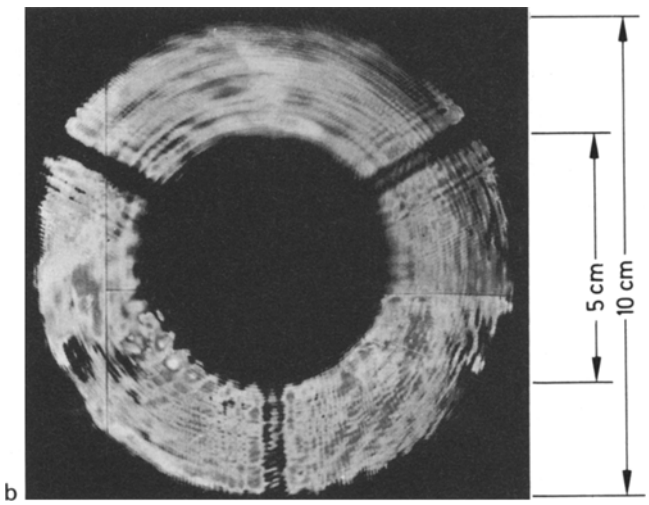

Fig. 3. (a) Energy profile of the CO_2-laser emission in the focal plane of a $f=714$ mm-lens after Handke [5b, 8b]. This far-field distribution showing a central maximum and several minima must be expected from the diffraction limited focussing of the near-field distribution of (b). Circles are infra-red camera measurements, crosses are taken from polaroid exposures. (b) Near-field distribution of CO_2-laser emission (polaroid exposure) after Handke [5b, 8b]

time averaged temperatures of $k_B T_i \approx k_B T_e \approx 10$ eV. It was a fully ionized hydrogen plasma with negligible impurities and hence $Z=1$ which, for the purpose of this investigation, was kept at 0.16 critical density.

Particular care was also devoted to the CO_2-laser system shown in Fig. 1 to approach the stipulations of theoretical treatment. The main features of the master oscillator and the pulse cutting system were described in [10]. Operated in a self-locking mode it emitted a single TEM_{00}-$P(20)$ pulse of less than 2 ns duration. Via an SF_6 cell and an optical isolation set-up this pulse was fed into the unstable resonator of a 10-l

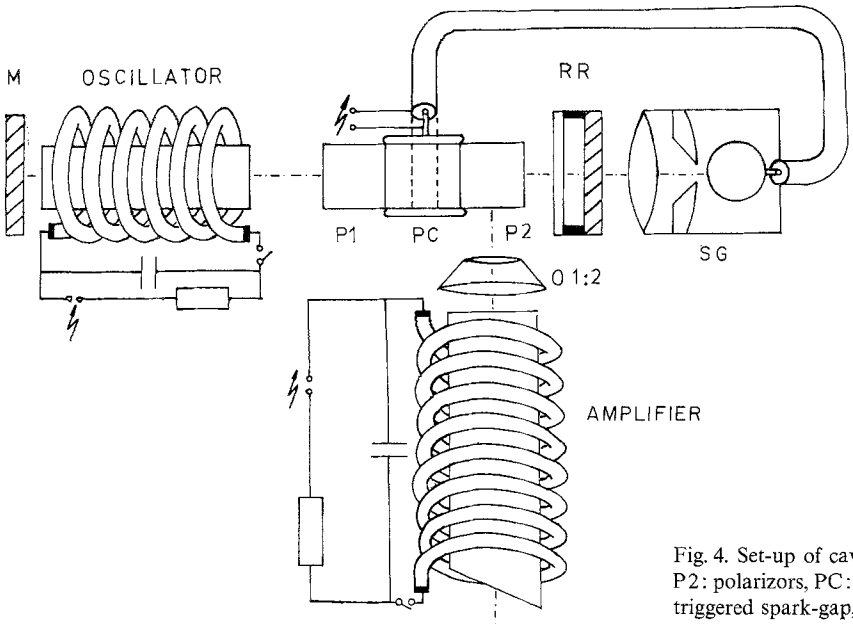

Fig. 4. Set-up of cavity dumped ruby laser-system (M: mirror, P1, P2: polarizors, PC: Pockels cell, RR: resonance reflector, SG: laser triggered spark-gap, O1:2: 1:2 beam expanding optics)

e-beam device. Thus modelocked, the amplifier emitted a train of pulses at 16.7 ns intervals which were reaching into the multi-Gigawatt range within one emission sequence (Fig. 2).

In order to provide for well-defined and reproducible laser conditions in the interaction volume the resonator was adjusted to emit in the fundamental mode with the annular near field of 10 cm outer diameter being focussed diffraction-limited by a lens of approximately 70 cm focal length to give an energy distribution in the beam waist, as it is visualized in Fig. 3. Details of the CO_2-laser system can be found in [8, 9a, 9c, 11].

As the diagnostic laser, a ruby-laser was used. In spite of the required powers of the order of 100 MW it did not heat the interaction volume markedly. The laser line-width was below 0.1 Å. Also, this choice of wavelength had the advantage that scattering spectra could easily be recorded with high time resolution by multichannel devices available in the visible wavelength region. In addition, the ruby-laser wavelength still permitted scattering to be detected under reasonable angles around 7^0. The ruby-laser used was a cavity dumped oscillator-amplifier system depicted in Fig. 4. One of the two plane mirrors of the oscillator was the usual resonance reflector to provide the narrow line-width emission. In order to obtain a short pulse of a few nanoseconds the 20% transmission of this reflector was used to trigger a spark gap (SG) at peak power. The voltage drop produced served to switch a Pockels cell (PC) which in turn "cavity dumped" [12] the radiation energy of the left resonator portion through the Glan-prisma P 2 to feed the amplifier. In a very conservative but reliable operation the system was made to emit up to 200 MW in a 5 ns pulse of about 2 mrad divergence angle. The pulse was focussed into the plasma by a biconvex lens of 1 m focal length.

In scattering by only the thermal density fluctuations of the plasma, one was faced with the problem of suppressing excessive spurious stray light originating from the primary laser beam. In order to avoid such interference with the measurements in case of the weak scattering by thermal density fluctuations, the ruby-laser beam was fed through the plasma via extensive aperture tubes and also the scattered light was accepted through such tubes constructed to dump stray light.

Another major problem for the light-scattering measurements arose from the need for synchronizing various complex system such as Z-pinch, CO_2 laser, ruby-laser and the gated detection system within nanoseconds. The inevitable jitter could not be brought down to below nanoseconds and, in order to obtain results during the 1–2 ns interaction of the CO_2-laser, measurements had to be repeated in sort of a trial and error method. To gain spectra on a shot by shot basis was, thus, impossible. Even though it had not been our intention, the use of an optical multichannel analyser (OMA) was mandatory. It is shown in Fig. 5.

The light accepted from the selected scattering volume in the plasma was imaged by an $f=0.5$ m lens into the 1 mm^2 input end of a glass-fibre bundle, the other end of which was shaped to act as the entrance slit of the spectrometer. This was a Littrow type device featuring a ruled Echélle grating of high diffraction order and an objective of large f-number. In this way a linear dispersion of 0.3 nm/mm was achieved resulting in a resolution of 0.007 nm/OMA channel. An image in-

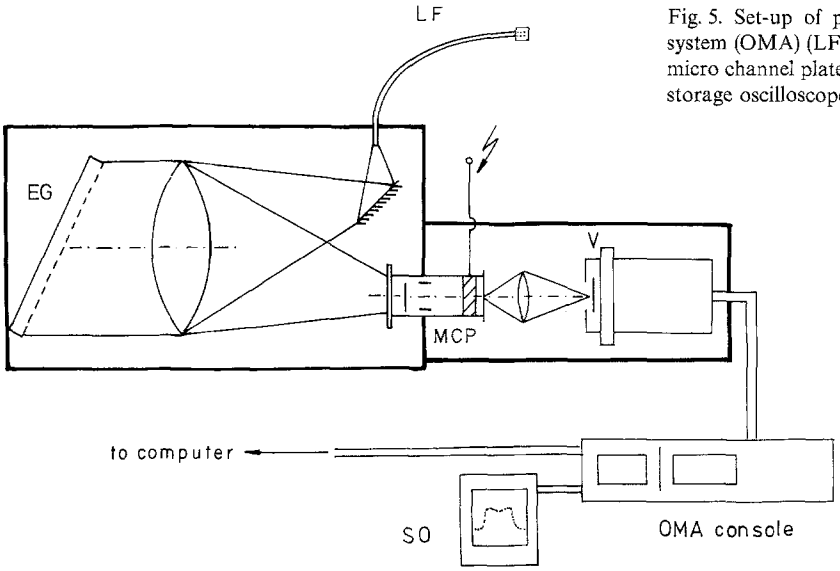

Fig. 5. Set-up of polychromator – optical multichannel analyzer system (OMA) (LF: light guiding fibre, EG: echélle grating, MCP: micro channel plate image intensify-tube, V: SIT-Vidikon tube, SO: storage oscilloscope)

tensifier MCP served to amplify the light-scattering spectra for recording by the multichannel device V and as a nanosecond shutter. Gating of the amplifying channelplate led to a transmission of the spectra within a 2.5 ± 0.2 ns interval only. In this way the time resolution of 5 ns given by the ruby-laser was improved. The spectra recorded could either be photographed from the screen of a storage scope or be transmitted by optical fibres to a PDP 11 computer for digital recording and processing. Alternating measurements without ruby-laser provided spectra of the plasma radiation required for subtraction from the light-scattering spectra and for calibration of wavelength channels.

2. Results

2.1. Diagnostics of the Target Plasma

Only space and time averaged values of electron and ion temperatures and density of the Z-pinch plasma were known from spectroscopical investigations [13]. By contrast, light-scattering can provide time resolved local plasma parameters. In a first attempt the radial distributions of the initial values of temperatures and density were measured in the particular plasma column crossection which was irradiated by the CO_2-laser. To minimize spurious stray light, scattering was observed at an angle of 93°.

The geometry chosen corresponds to a scattering parameter $\alpha \approx 6$ (collective scattering) according to (1)

$$\alpha = \frac{\lambda}{4\pi \sin(\theta/2)\lambda_D}, \tag{1}$$

where λ is the wavelength of incident radiation, λ_D the Debye length, and θ the scattering angle.

The arrangement of devices is displayed in Fig. 6. The collecting solid angle of lens L 3 amounted to 10^{-3} sr. The scattering volume was 6 mm^3. A signal to noise ratio of better then 5 : 1 was obtained. Total transmission of near 100% could be shown experimentally and negligible heating of the plasma due to inverse "bremsstrahlung" absorption was estimated. Further detailed estimates of scattering properties are given in [9a, 9c].

An example of the light-scattering spectra as they were obtained on the readout screen is given in Fig. 7a, whereas Fig. 7b visualizes the spectrum after application of relative calibration and representing three adjacent channels by one experimental point. The full drawn narrow line represents the ruby-laser line being mainly broadened by the apparatus profile. In order to evaluate plasma parameters from these curves, theoretical spectra according to [14] were convoluted with this apparatus profile for parameters estimated in a first step. In comparing experimental and such convoluted spectra in a nonlinear best fit regression code, up to six independent plasma parameters were obtained including the confidence intervals of the nonlinear regression parameters. The numerical method, which is described in [9a, 9c] makes use of a steepest gradient descent algorithm of rather slow convergence and switches to a fast Newton-like algorithm after a few iterations had been successful. The procedure is based upon the algorithm of Marquardt [15]. The dashed curve of Fig. 7b is such a best fit spectrum. It corresponds to the following set of plasma parameters $k_B T_e = (12.4 \pm 0.7)$ eV, $k_B T_i = (10.0 \pm 0.9)$ eV and drift velocities of electrons and ions $v_{De} = (-1.5 \pm 5.2)\ 10^4$ m/s, $v_{Di} = (-7.3 \pm 1.9)\ 10^3$ m/s. The numerical error of the electron drift velocity shows that this

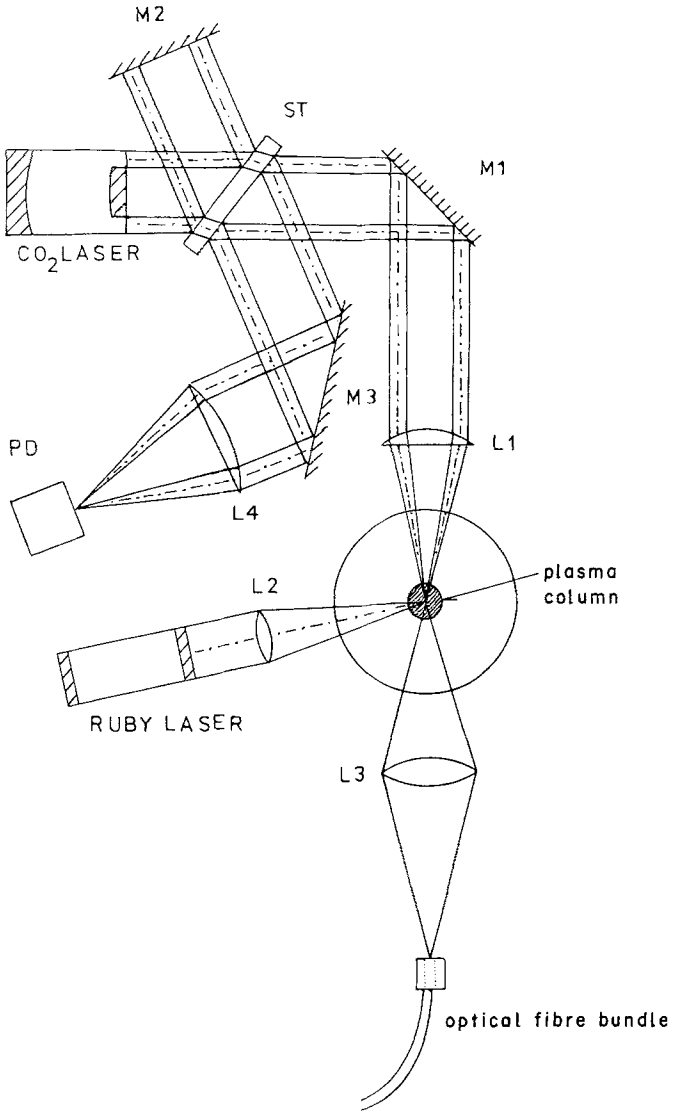

Fig. 6. Experimental arrangement of 93° Thomson scattering experiment during CO_2-laser irradiation (M1, M2, M3: mirrors, ST: beam splitter, L1, L2, L3, L4: lenses, PD: photon drag detector)

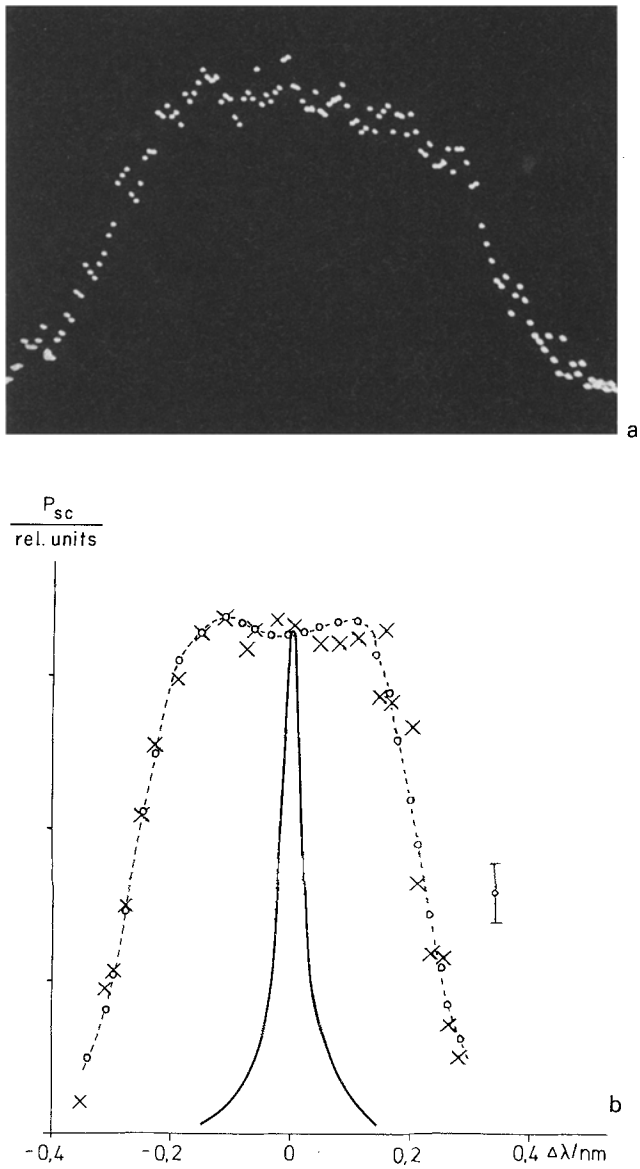

Fig. 7. (a) Typical 93° light-scattering spectrum photographed from the readout screen of the OMA system. (b) Spectrum of (a) after considering calibration of different channels. Three adjacent channels are represented by one experimental point (indicated as cross). The full drawn curve shows the incident ruby-laser line, whereas the dashed line is a nonlinear best fit to the experimental points corresponding to the plasma parameters: $k_B T_e = (12.4 \pm 0.7)$ eV, $k_B T_i = (10.0 \pm 0.9)$ eV, $v_{De} = (-1.5 \pm 5.2) 10^4$ m/s, $v_{Di} = (-7.3 \pm 1.9) 10^3$ m/s

value is small and not significant. Even though this particular spectrum was obtained at the end of the 80 ns resting phase of the plasma during which measurements were performed throughout, the above ion drift velocity was very small compared to thermal velocities. Thus plasma dynamics could be neglected in the initial interaction conditions.

From the multitude of scattering data sets obtained over many shots for the whole range of plasma radii, it appears that temperatures were evenly distributed over the 18 mm diameter plasma column. Temperatures averaged over many shots varied in the range $k_B T_e = (11 \pm 3.5)$ eV and $k_B T_i = (10.5 \pm 1.5)$ eV. By making use of the wavelength integrated total scattering intensity the relative density distribution across radius could be determined as well. A few experimental values are plotted in Fig. 8. The dashed curve indicates the values derived by spectroscopical means [13b]. The homogeneous extension over about 7 mm in radius is confirmed. Only the drop to larger radii seems to have been seen with greater spatial resolution by the light-scattering measurements. Also, the absolute values of the homogeneous portion of density distribution are confirmed reasonably well. In fact, the errors indicated

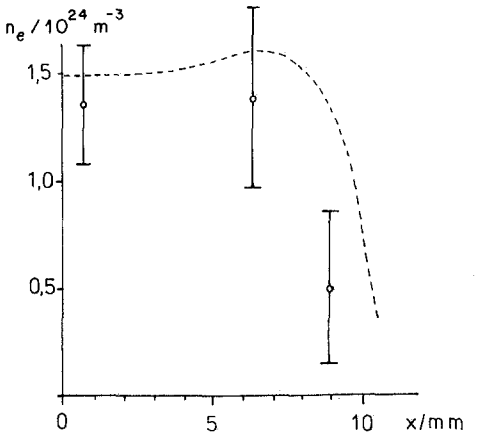

Fig. 8. Plasma density distribution. Experimental values were taken from measurements of wavelength integrated total scattering intensity. The dashed line shows the density distribution measured spectroscopically [13b]

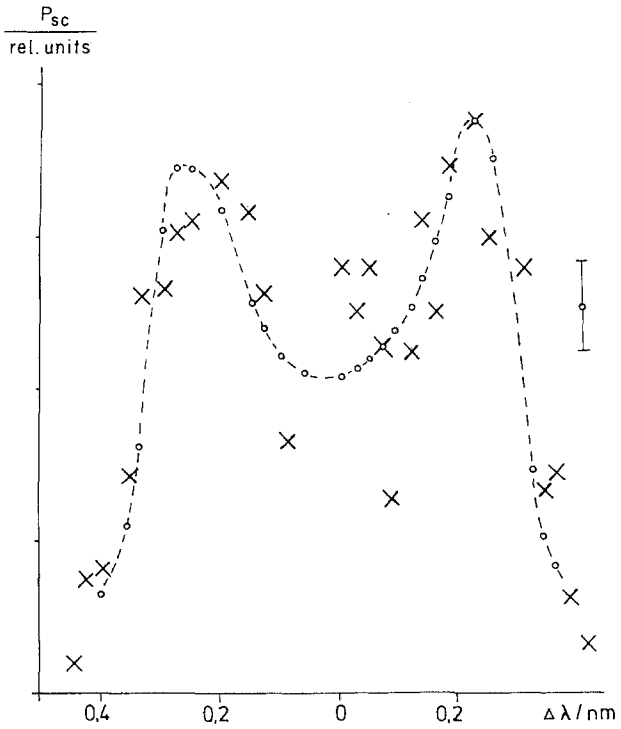

Fig. 9. Typical example of a 93° light-scattering spectrum, when the CO_2-laser was incident. Three adjacent channels are represented by one experimental point (indicated as cross). The dashed line is a nonlinear best fit to the experimental points corresponding to the plasma parameters: $k_B T_e = (38.6 \pm 3.9)$ eV, $k_B T_i = (12.2 \pm 0.8)$ eV, $v_{De} = (3.5 \pm 9.9) 10^4$ m/s, $v_{Di} = (-5.0 \pm 2.6) 10^3$ m/s

in Fig. 8 are absolute errors. The relative errors in particular those of a single shot are actually less.

Of course, of actual interest were the plasma parameters during interaction with the CO_2-laser radiation. The respective light-scattering measurements were performed in the same arrangement of Fig. 6. For each light-scattering spectrum the time dependence of incident CO_2-laser power and backscattered SBS power was recorded on a fast oscilloscope by one and the same detector PD. The laser signal split off by beam splitter (BS) was delayed appropriately against the SBS signal which was reflected onto PD by the same beam splitter. Finally, by adjusting optical paths and signal cable lengths, the time dependence of ruby laser irradiation and OMA gating could be recorded on the same oscilloscope trace, in this way permitting to determine the temporal correlation of the various processes within about 0.5 ns. Thus, measuring on a trial and error basis, scattering spectra were obtained for any degree of coincidence. Well correlated with the degree of coincidence the spectra displayed an increase in width and the appearance of pronounced humps an example of which is plotted in Fig. 9.

As in Fig. 7b experimental points (crosses) represent the mean values of each three adjacent wavelength channels and the dashed curve shows the best fitting spectrum. Obtained about 1 ns after CO_2-laser peak power the expected rise in electron temperature is confirmed, whereas an eventual laser-induced drift motion must be negligible by comparison with thermal velocities. In addition, the small drift indicated in the ion drift velocity corresponds to the rudimentary plasma dynamics both in direction and magnitude.

A large number of spectra was obtained covering wide ranges in laser power and time delay between CO_2-laser and measurement of such plasma parameters.

With the aim of having ready at hand this extensive data material it was tested wether this behaviour of plasma parameters could be described by the heating model developed and confirmed in several aspects in [7, 8].

This model uses linear inverse "bremsstrahlung" absorption in the interaction volume and Spitzer heat conduction in the established temperature gradient to carry away the heat produced. Because of its extensive description [8] we must not go into details of formulations. However, since we are interested to describe temperature behaviour also several nanoseconds after CO_2-laser irradiation, heat transfer to ions must be included here and even heat conduction by ions. Besides, another difference to the applications in [8] arises from the fact that light-scattering spectra are observed from a larger diameter than the central peak in the focal distribution of the CO_2-laser (Fig. 3). For averaging purposes the radial distributions of temperatures must be known. This would have required to start the computer run with the exact focal distribution. Numerical calculations, however, showed that already 200 ps after the beginning of the 2 ns laser pulse the ring shaped distribution according to Fig. 10 was smeared out and a monotonic profile-such as curve B –

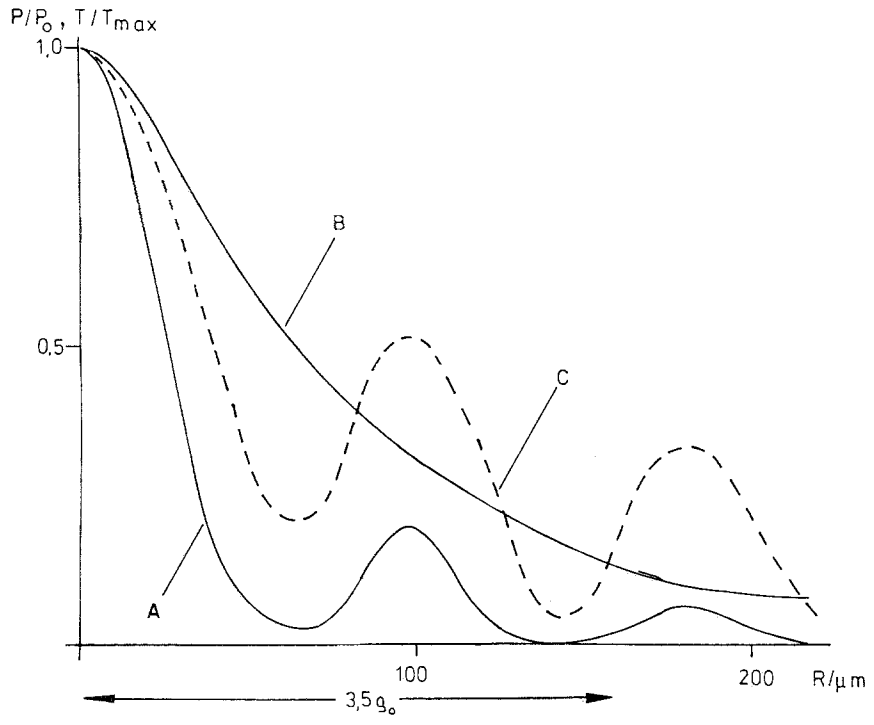

Fig. 10. Normalized energy distribution of CO_2-laser radiation P/P_0 (Curve A, P_0: maximum intensity in the centre) in the focal plane of a $f=714$ mm lens according to Handke [5b, 8b]. Curve B shows an approximation for the corresponding temperature profile C

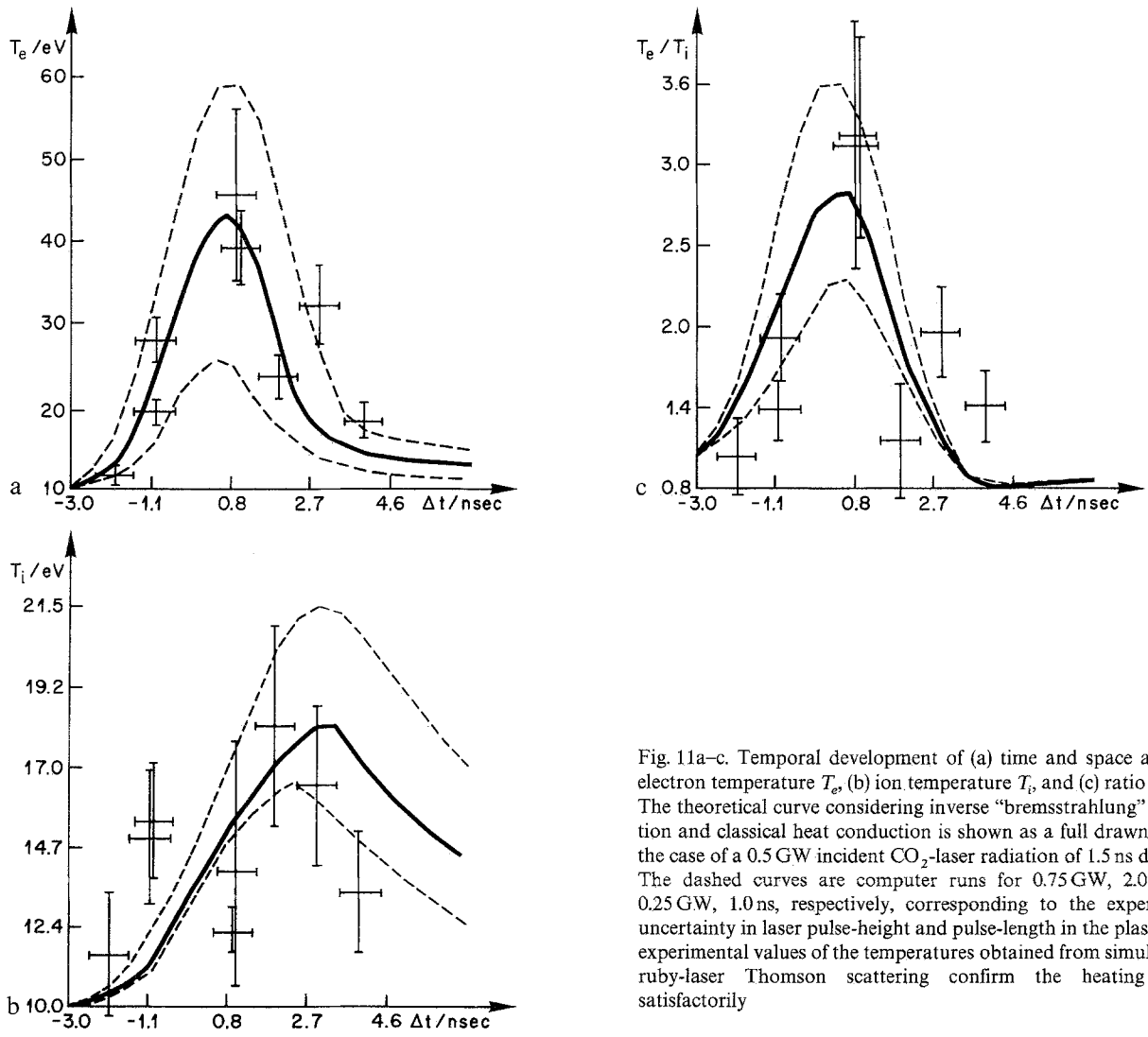

Fig. 11a–c. Temporal development of (a) time and space averaged electron temperature T_e, (b) ion temperature T_i, and (c) ratio of T_e/T_i. The theoretical curve considering inverse "bremsstrahlung" absorption and classical heat conduction is shown as a full drawn line for the case of a 0.5 GW incident CO_2-laser radiation of 1.5 ns duration. The dashed curves are computer runs for 0.75 GW, 2.0 ns, and 0.25 GW, 1.0 ns, respectively, corresponding to the experimental uncertainty in laser pulse-height and pulse-length in the plasma. The experimental values of the temperatures obtained from simultaneous ruby-laser Thomson scattering confirm the heating model satisfactorily

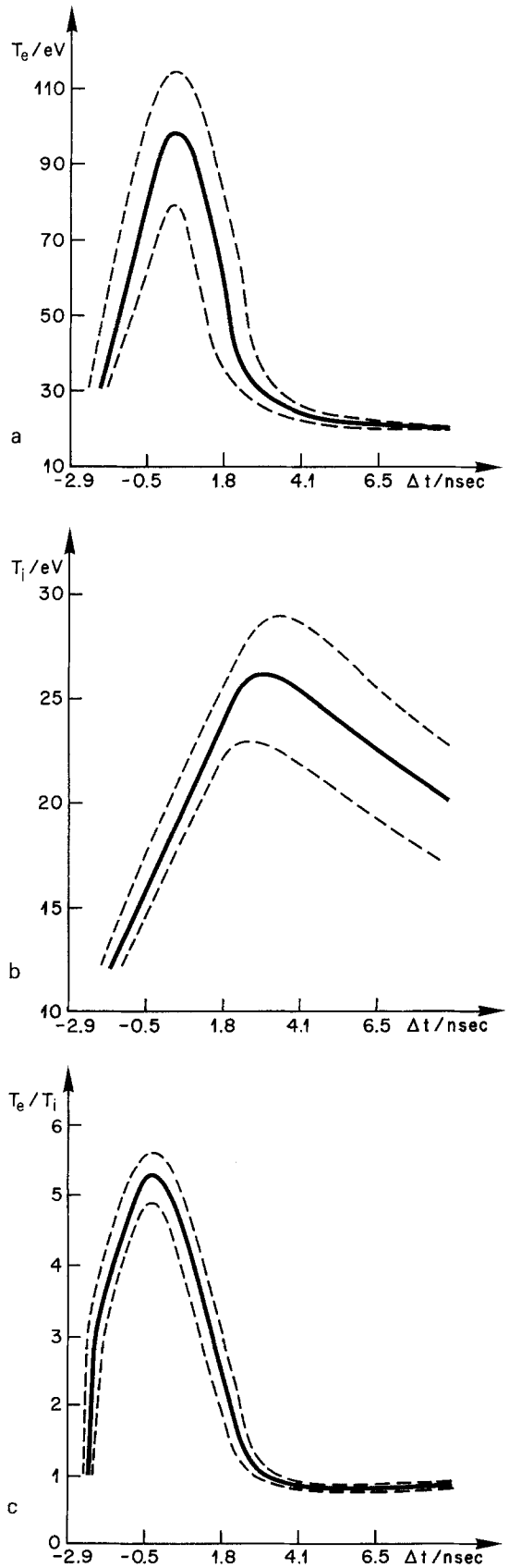

Fig. 12a–c. Time dependence of non averaged (a) electron temperature T_e, (b) ion temperature T_i, and (c) ratio T_e/T_i derived from Fig. 11

was describing the temperature distribution sufficiently well.

In addition to forming radial averages of temperatures for the comparison with light-scattering values, also time averages had to be formed in order to account for the fact that they were measured for 2 ns periods. The computed temperature values to be compared with the experimental values, thus, were space and time averaged values. In order to make sure that these mean values were still representative for the narrow SBS volume rather than for the surrounding plasma the averages were formed for various diameters and so were measurements performed by using apertures of different diameters in front of the accepting glass-fibre bundle of Fig. 5. The comparison showed agreement between computed and experimental temperatures and revealed that these average values were representing that of the narrow SBS volume, the reason being the extremely rapid spread of elevated temperatures. The integrals to be solved were computed by usual Newton-Cotes-quadrature procedure with an error limit of 10^{-4}.

Figure 11a–c, finally show the time dependence of the above temperature mean values and their ratios. In order to account for experimental uncertainties in CO_2-laser intensity of about $\pm 40\%$ and time coincidence of ± 0.5 ns three curves are plotted in between which the experimental points should come to lie. The comparison shows a very satisfying confirmation of the behaviour of electron temperature. In case of the ion temperature the agreement is still reasonable, in particular, since here changes in the initial plasma temperature make themselves felt with greater weight. The deviation of points at -1.1 ns could be traced to such reasons. Finally, the evaluation of spectra obtained about 10 ns after CO_2-laser irradiation showed that not only T_e/T_i had tapered off to unity but that T_e and T_i also had approached closely the initial values. At 16.7 ns when the subsequent CO_2-laser pulse arrived the plasma could be assumed safely to pose nearly identical conditions for the interaction. This justifies the evaluation of parameters from subsequent SBS pulses of a pulse train such as has been done in [7, 8, 11]. The time dependence of non averaged temperatures in the SBS volume which can be derived from the above measurements are plotted in Fig. 12a–c.

The onset of SBS from the turbulence enhanced or thermal level is still under discussion [3a, 3b]. The fact, that the scattering spectra could be fitted so well to that of a thermal plasma implies that scattering had occured on thermal density fluctuations only and the CO_2-laser interaction had not produced enhanced density fluctuations at the wave number of the scattering vector. It is, therefore, not likely that some sort of turbulent microfields were created within, and in the

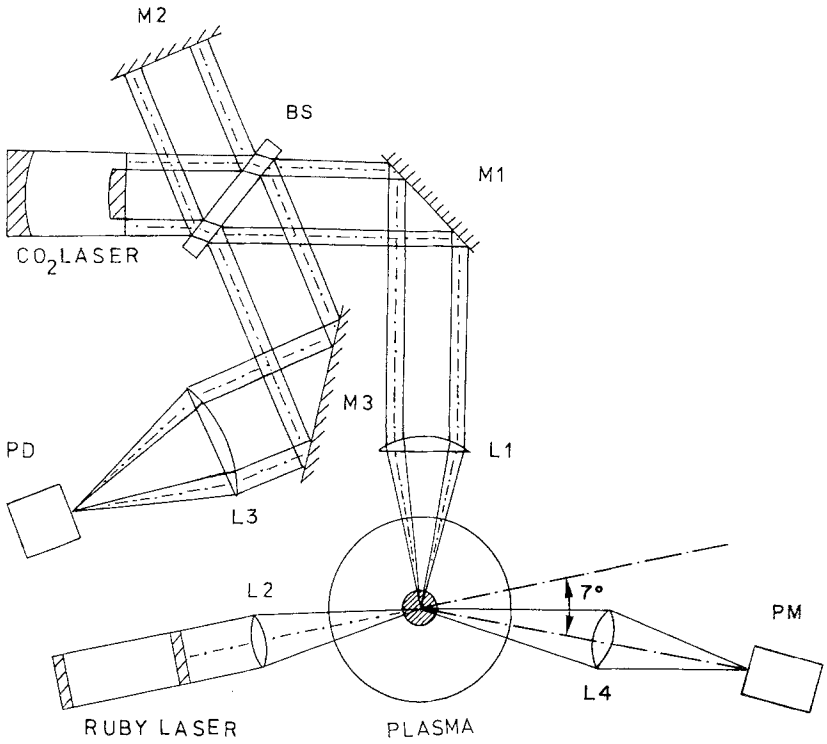

Fig. 13. Experimental arrangement for the investigation of ion acoustic wave amplitudes (M1, M2, M3: mirrors, BS: beam splitter, PD: photon drag detector, PM: photomultiplier or vacuum photodiode)

vicinity of the interaction volume which could have impeded heat conduction. This statement again is in agreement with the fact that unimpeded classical heat transfer in the heating model was capable to describe the temperature behaviour above and near SBS threshold [8].

2.2. *Light Scattering Investigations at the Wave-Vector of the* SBS *Ion Acoustic Wave*

In order to obtain light-scattering from a wave-vector corresponding to that of the backscattering ion acoustic wave $\mathbf{k}_{ia} \approx 2\mathbf{k}_0$($\mathbf{k}_0$ wave-vector of CO_2-laser beam), the scattering angle had to be reduced to about 7° in the set-up of Fig. 6 to meet the light scattering condition (Fig. 14b)

$$\mathbf{k}_{ia} = \mathbf{k}_{sc} - \mathbf{k}_{\text{rub}}. \tag{2}$$

This is shown in Fig. 13.

Level of Density Fluctuation Before CO_2*-Laser Irradiation.* After it had been checked that light-scattering spectra obtained at 7° revealed essentially the same plasma conditions as those measured at 93°, the OMA system was replaced by an high-sensitivity photomultiplier of nanosecond time resolution. Thanks to refined aperture tubes the spurious stray light level was negligible and the photomultiplier signals represented the wavelength integrated scattering intensity accepted from the scattering volume. As a consequence of extreme forward scattering, the rhombic light-scattering volume was by more than two orders of magnitude larger than the SBS volume contained in it. It is for this reason, that the observation of mere thermal scattering from this larger volume did not permit us to conclude the same for the level of density fluctuations or coherent modulations in the small SBS region. It was the finite error in the absolute level of density fluctuations of the much larger light-scattering volume which prevented us from pinning down this level in the SBS volume to below ten times thermal. By contrast, 93°-light-scattering could be selected to originate mainly from the SBS volume by putting a scanable aperture in front of the accepting glass-fibre bundle of Fig. 5. In this way it was possible to state that, during CO_2-laser irradiation, density fluctuations at $k_{93°}$ are of thermal level only. Since $k_{93°}$ was small compared to the reciprocal Debye length it must be inferred that no kind of strong turbulence existed in the plasma. It is, therefore, unlikely that suprathermal density fluctuations prevailed at $k_{7°}$. Further support for this statement comes from the measurement of SBS growth by means of subnanosecond streak camera [9a] and 100 ps-detectors [7]. These measurements extrapolated to the time of threshold indicate near thermal initial amplitudes of the SBS instability.

Density Modulation During SBS*-Occurence.* In scattering from the density modulation of the backscattering

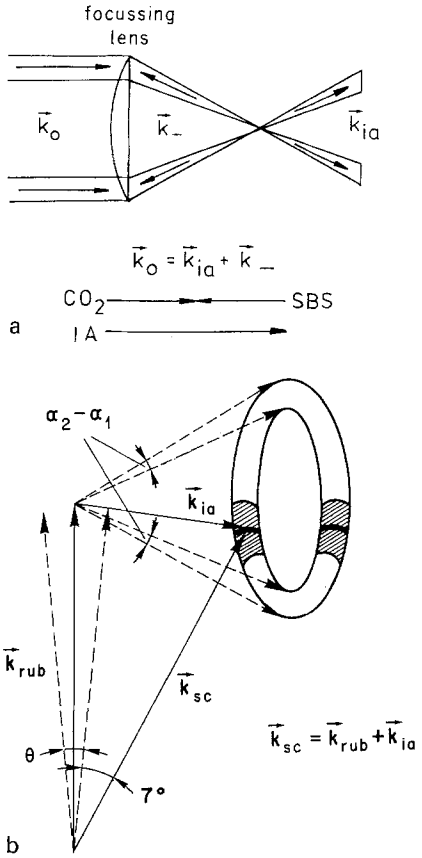

Fig. 14. (a) Wave-vector diagram of the SBS process. The annular CO_2-laser radiation ($\mathbf{k}_0$) is focussed into the plasma giving rise to ion acoustic waves ($\mathbf{k}_{ia}$) and backscatter ($\mathbf{k}_-$). (b) Wave-vector diagram of the Thomson scattering process. The incident ruby laser radiation ($\mathbf{k}_{rub}$) is scattered at the SBS excited ion acoustic wave ($\mathbf{k}_{ia}$) and recorded in the $\mathbf{k}_{sc}$-direction. The phase matching condition $\mathbf{k}_{sc} = \mathbf{k}_{rub} + \mathbf{k}_{ia}$ is only fulfilled for those vectors $\mathbf{k}_{sc}$ lying on the full drawn line of the tire shaped ring. This line is smeared out (shaded area) because of the spread in incidence angle $\alpha_2 - \alpha_1$ and the divergence of the laser beams

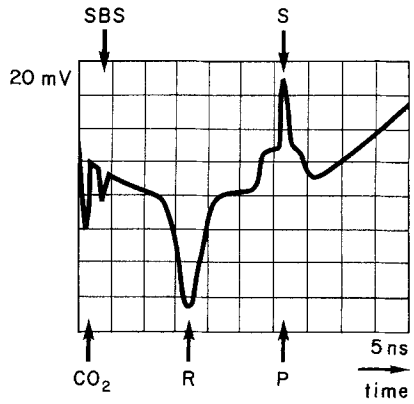

Fig. 15. Addition of various monitors leads to the oscilloscope trace shown. Considering different time delays in the recording arrangement the ruby-laser radiation "R" and CO_2-laser radiation "CO_2" are incident on to the same plasma region at the same time. In such a case a scattering signal "S" on the reference pedestal "P" (see text) is monitored arising from scattering at the highly excited ion acoustic wave of the SBS process. "SBS" is the backscattered infra-red radiation

ion acoustic wave, a distinct difference to light-scattering on thermal density fluctuations arises here from the situation, that the above wave-vector condition must be met for a quite specific $\mathbf{k}_{ia}$, the little leeway in alignment being given only by the divergence angles of the ruby-laser beam and the spread $\alpha_2 - \alpha_1$, in the $\mathbf{k}_{ia}$-distribution indicated in Fig. 14b. Due to the conical far-field pattern of the CO_2-laser beam, ion acoustic waves of wave vector $\mathbf{k}_{ia} \approx 2\mathbf{k}_0$ ($\mathbf{k}_0$ wave-vector of CO_2-laser beam) only existed for the conical distribution visualized in Fig. 14b. In this figure, also the tire shaped range in k-space is drawn, within which the scattering wave-vector must be chosen to observe scattering by the ion acoustic wave stimulated in SBS. Contrary to usual light-scattering techniques this required careful scans to find coincidence.

This light-scattering then exhibited the same rise above thermal level as it is observed in SBS. Because of its large magnitude it could be detected even with fast photodiodes. Figure 15 shows such a signal S the temporal development of which closely corresponds to that of the SBS signal. In order to visualize the degree of coincidence with the ruby-laser power the spurious stray-light level had been increased deliberately to form a reference pedestal. Onto the same trace of a 300 ps oscilloscope the CO_2-laser power (CO_2), the corresponding SBS signal (SBS), and the ruby laser power (R) were added with well-known time delays to provide synchronisation and calibration references.

In order to obtain values of the relative density modulation of the backscattering ion acoustic wave $\delta n_{ia}/n_e$ a number of correction factors must be considered. First, because of the conical distribution of $\mathbf{k}_{ia}$ the wave number conditions for light-scattering could be met only for the shaded portion of the k-space region of $\mathbf{k}_{ia}$ in Fig. 14. Second, the fraction of scattering volume occupied by the SBS ion acoustic wave had to be accounted for. Its length was known from streak-camera measurements of the SBS volume [9a] and its cross-section from the focal diameter of the CO_2-laser beam from which SBS was observed. Third, since the ruby-laser illumination of the large plasma cross-section was not homogeneous, another correction had to be applied for different positions of the SBS volume in the plasma. Fourth, the total time response of the detection system was not much faster than the scattering pulse; therefore pulse height had to be corrected accordingly. Fifth, in quoting an enhancement above thermal density fluctuations the differing spectral distribution was to be accounted for. Because of its narrow width only the spectrally integrated power was measured with scattering from the SBS ion acoustic

wave. For the purpose of forming a correction factor, its width was estimated from time broadening, only. Sixth, scattering occurred on a coherent wave rather than by the statistical density fluctuations of a thermal plasma, i.e., the scattering intensity was given by the squared sum of all scattering amplitudes rather than by the usual sum of their squares. The relation required could be derived from the system of coupled-wave equations describing the SBS process itself [1]. Neglecting dispersion and damping of the electromagnetic waves this nonlinear system can be solved analytically to give the normalized scattering power for conditions well below unity in steady-state approximation (see e.g. [9a, 9c] or [18] as

$$\frac{P_{sc}}{P_0} = \tanh^2(\beta L), \tag{3}$$

where

$$\beta = \frac{\omega_{pe}^2}{4c^2 k_{\mathrm{rub}}} \frac{\langle \delta n_{ia} \rangle_x}{n_e}. \tag{4}$$

P_{sc} is the scattered power, P_0 the ruby-laser power (homogeneous illumination of scattering volume), L the length of scattering coherent wave, ω_{pe} the electron plasma frequency, c the velocity of light, k_{rub} the ruby-laser wave-vector, $\langle \delta n_{ia} \rangle_x$ the density amplitude of scattering wave averaged over propagation direction x, and n_e the electron number density.

From this relation the important interaction parameter

$\frac{\langle \delta n_{ia} \rangle}{n_e}$ (δn_{ia} density amplitude of the backscattering ion acoustic wave)

could be evaluated, if the above correction factors are applied and if only wavelength, i.e. frequency integrated light-scattering measurements were performed. Since this same basic relationship holds both for backscattering and ruby-laser light scattering, it is clear that both signals must have shown the same time development of normalised scattering power and the same quantity

$$\frac{\langle \delta n_{ia} \rangle}{n_e}$$

must have resulted from both measurements. The comparison confirmed this.

By means of a scanable narrow slit in front of the detecting photomultiplier or the planar diode, it was possible to select scattering from the SBS volume and from volumes immediately adjacent to it. Whilst scattering from the narrow interaction volume exhibited the referred coincidence in temporal evolution and enhancement, immediately adjacent regions did not reveal any increase above thermal scattering. For the aforementioned reasons this means that across one diameter from the SBS region the greatly enhanced density modulations had dropped to below ten times thermal. Obviously, the level of density modulations in the SBS region was not high enough to create wave-number components via some nonlinear mechanism that had propagated into the adjacent plasma.

3. Summary

In concluding, we have demonstrated by ruby-laser light-scattering techniques that our computer refined heating model [8] is capable to describe plasma parameters under the influence of CO_2-laser irradiation correctly. By the same means upper limits could be established for the initial amplitude of the backscattering ion acoustic wave. In addition, it was demonstrated that backscattering and ruby-laser light-scattering lead to the same values of density modulation of the enhanced ion acoustic wave. Also the existence of possibly turbulence-enhanced density fluctuations at the investigated wave numbers in the SBS volume and adjacent to it can be excluded. This supports from a quite different angle of view the observation of earlier work [8a] that heat conduction in model plasmas of this kind can be described by the classical formulation of Spitzer [16] and Spitzer and Härm [17].

It is in this way that by the above work the experimental groundwork is now laid for the attempt to interpret extensive light-scattering measurements of various SBS aspects in terms of existing theoretical treatments.

Acknowledgements. We should like to thank our colleagues Drs. J. Handke and S. A. H. Rizvi for cooperation and Dr. D. Rusbüldt for providing valuable hardware. Our appreciation for discussions on theoretical matters with Prof. Dr. H. Schamel must also be expressed here. The work of Mrs. Zamfirescu, who prepared the figures with great skill, is gratefully acknowledged. This work was performed under the auspices of the "Sonderforschungsbereich No. 162, Plasmaphysik Bochum/Jülich".

References

1. D.W. Forslund, J.M. Kindel, E.L. Lindmann: Phys. Fluids **18**, 1002–1016 (1975)
2. a) A.A. Offenburger, A.Ng.M.R. Cervenan: Can. J. Phys. **56**, 381–386 (1978)
   b) A. Ng, A.A. Offenberger, S.J. Karttunen: Opt. Commun. **36**, 200–204 (1981)
   c) A. Ng, L. Pitt, D. Salzmann, A.A. Offenberger: Phys. Rev. Lett. **42**, 307–311 (1979)
3. a) M.J. Herbst, C.E. Clayton, F.F. Chen: Phys. Rev. Lett. **43**, 1591–1595 (1979)
   b) J.J. Turecheck, F.F. Chen: Phys. Fluids **24**, 1126–1141 (1981)
   c) C.E. Clayton, C. Joshi, A. Yasuda: F.F. Chen: Phys. Fluids **24**, 2312–2318 (1981)

4. a) R.S. Massey, Z.A. Pietrzyk, D.W. Scudder: Phys. Fluids **21**, 396–403 (1978)
b) R.S. Massey, K. Berggren, Z.A. Pietrzyk: Phys. Rev. Lett. **36**, 963–965 (1976)
c) Z.A. Pietrzyk, T.N. Carlstrom: Appl. Phys. Lett. **35**, 681–683 (1979)
5. a) F.F. Chen: Proc. Intern. Conf. on Plasma Physics, Vol. II, (1980) p. 345
b) J. Handke: Dissertation, Physics and Astronomy Department, Ruhruniversität, D-4630 Bochum, Fed. Rep. Germany (1982)
c) J. Handke, S.A.H. Rizvi, B. Kronast: Phys. Rev. Lett. (submitted)
6. F.J. Mayer, A.E. Busch, C.M. Kinzer, K.G. Estabrook: Phys. Rev. Lett. **44**, 1498–1501 (1980)
7. J. Handke, S.A.H. Rizvi, B. Kronast: Appl. Phys. **25**, 109–113 (1981)
8. a) J. Handke, S.A.H. Rizvi, B. Kronast: Laser and Particle Beams (August 1983)
b) J. Handke: Report 82-N3-108 (1982) Sonderforschungsbereich 162, Plasmaphysik Bochum/Jülich, Ruhruniversität, D-4630 Bochum, Fed. Rep. Germany
c) B. Gellert, J. Handke: Comp. Phys. Commun. **30** (1983)
9. a) B. Gellert: Report 82-N3-109 (1982) Sonderforschungsbereich 162, Plasmaphysik Bochum/Jülich, Ruhruniversität, D-4630 Bochum, Fed. Rep. Germany
b) B. Gellert, B. Kronast: Appl. Phys. (submitted)
c) B. Gellert: Dissertation, Physics and Astronomy Department, Ruhruniversität, D-4630 Bochum, Fed. Rep. Germany (1982)
10. B. Gellert, J. Handke, B. Kronast: Appl. Phys. **19**, 257–264 (1979)
11. S.A.H. Rizvi: Dissertation, Physics and Astronomy Department, Ruhruniversität, D-4630 Bochum, Fed. Rep. Germany (1983)
12. a) J. Ernest, M. Michon, J. Debrie: Phys. Lett. **22**, 147–149 (1966)
b) W.R. Hook, R.H. Dishington, R.P. Hilberg: Appl. Phys. Lett. **9**, 125–127 (1966)
13. a) K.H. Finken, G. Bertschinger, S. Maurmann, H.J. Kunze: J. Quant. Spectrosc. Radiat. Transf. **20**, 467–476 (1978)
b) G. Bertschinger: Report KFA-IPP-IB-3/80, Inst. für Plasmaphysik der KFA Jülich, D-5170 Jülich, Fed. Rep. Germany (1980)
14. a) E.E. Salpeter: Phys. Rev. **120**, 1528–1535 (1960)
b) M.N. Rosenbluth, N. Rostoker: Phys. Fluids **5**, 776–788 (1962)
15. D.W. Marquardt: J. Soc. Ind. Appl. Math. **11**, 431–441 (1963)
16. L. Spitzer, Jr.: *Physics of Fully Ionized Gases* (Interscience, New York, 1956)
17. L. Spitzer, Jr. R. Härm: Phys. Rev. **89**, 977–981 (1952)
18. W.L. Kruer: Phys. Fluids **23**, 1273–1275 (1980)